High-Precision 5DoF Tracking and Visualization of Catheter Placement in EVD of the Brain Using AR

XUETONG SUN, University of Maryland College Park
SARAH B. MURTHI and GARY SCHWARTZBAUER, University of Maryland School of Medicine
AMITABH VARSHNEY, University of Maryland College Park

9

External ventricular drainage (EVD) is a high-risk medical procedure that involves inserting a catheter inside a patient's skull, through the brain and into a ventricle, to drain cerebrospinal fluid and thus relieve elevated intracranial pressure. Once the catheter has entered the skull, its tip cannot be seen. The neurosurgeon has to imagine its location inside the cranium and direct it toward the ventricle using only anatomic landmarks. The EVD catheter is thin and thus hard to track using infra-red depth sensors. Traditional optical tracking using fiducial or other markers inevitably changes the shape or weight of the medical instrument. We present an augmented reality system that depicts the catheter for EVD and a new technique to precisely track the catheter inside the skull. Our technique uses a new linear marker detection method that requires minimal changes to the catheter and is well suited for tracking other thin medical devices that require high-precision tracking.

CCS Concepts: • **Computing methodologies → Tracking**; • **Human-centered computing → Mixed / augmented reality**;

Additional Key Words and Phrases: Augmented reality, 5DoF tracking, external ventricular drain, assisted surgery, catheter placement

ACM Reference format:
Xuetong Sun, Sarah B. Murthi, Gary Schwartzbauer, and Amitabh Varshney. 2020. High-Precision 5DoF Tracking and Visualization of Catheter Placement in EVD of the Brain Using AR. *ACM Trans. Comput. Healthcare* 1, 2, Article 9 (March 2020), 18 pages.
https://doi.org/10.1145/3365678

1 INTRODUCTION

Catheter placement for external ventricular drainage (EVD) involves inserting a very small clear plastic tube into a lateral ventricle of the brain. Once the catheter is inside the skull, its position can no longer be directly observed,

This work was supported in part by NSF grants 18-23321, 16-32976, 15-64212, and 14-29404, and the State of Maryland's MPower initiative. Any opinions, findings, conclusions, or recommendations expressed in this article are those of the authors and do not necessarily reflect the views of the research sponsors.
Authors' addresses: X. Sun, University of Maryland College Park, 3104 Brendan Iribe Center, 8125 Paint Branch Drive, College Park, MD 20740; email: xtsun@umiacs.umd.edu; S. B. Murthi, University of Maryland School of Medicine, 901 Hillstead Drive, Lutherville, MD 21096; email: smurthi@umm.edu; G. Schwartzbauer, University of Maryland Medical Center Department of Neurosurgery, Suite 12D, Baltimore, MD 21201; email: GSchwartzbauer@som.umaryland.edu; A. Varshney, University of Maryland College Park, 3212 Brendan Iribe Center, 8125 Paint Branch Drive, College Park, MD 20740; email: varshney@umiacs.umd.edu.

2637-8051/2020/03-ART9 $15.00
https://doi.org/10.1145/3365678

and the neurosurgeon must rely on his or her experience and knowledge of human anatomy to guide placement of the catheter. Huyette et al. [2008] and Kakarla et al. [2008] retrospectively assess the accuracy of ventriculostomy catheter placement by comparing postprocedure CT scans with preoperative scans. The former study includes 98 ventriculostomy catheter placements and finds that in the authors' institution, it requires on average two passes to successfully place the catheter, and 22.4% of those successful placements end up in nonventricular spaces. The latter includes studies of 346 patients and finds that 13% of the catheter placements are suboptimal, resulting sometimes in unfunctional drainage. Furthermore, Woo et al. [2019] find that catheter misplacement is a significant independent predictor of catheter-associated hemorrhage. In a radiographic simulation, Robertson et al. [2017] find that the traditional method of EVD trajectory selection and placement is predicted to have a 19% chance to impact a cortical vein. These results show that there is still much room for improvement. A method of visualizing the location of the catheter inside the skull would be of great assistance to the surgeon.

A few EVD visualization techniques have been proposed. Cutler et al. [2017] have developed a system in which an optical marker is attached to the catheter and tracked by the camera on a head-mounted display (HMD). Other medical instrument tracking tehniques by Low et al. [2010], Najafi and Rohling [2011], Najafi et al. [2015], Stolka et al. [2014], and Fan et al. [2017] make use of markers of different kinds.

Microsoft Kinect has been successfully used to reconstruct 3D meshes representing humans at real-time rates [Du et al. 2019]. However, our preliminary tests with Microsoft Kinect 2.0 showed that the thinness of the catheter makes it hard to detect and track with commodity depth sensors. The shortcomings of infrared depth sensing, in this case, are outside the scope of this work.[1] Instead, we devise a new optical marker and tracking technique, suitable for augmented reality (AR). We label a portion of the catheter with three distinct colors. One design principle we have observed after consulting our medical collaborators is making minimal changes to the catheter. Our modification does not change the catheter in any way that would make it feel different to operate. We develop an algorithm to detect the color bands and then use them to calculate the position of the catheter. This way, even if the tip of the needle is occluded, we still know where it is and are able to visualize it, as long as enough of the colored portion remains visible. We display a virtual catheter overlaid on the real catheter directly in the user's field of view using a see-through Microsoft HoloLens, which allows the surgeon to better focus on the patient while still having access to the relevant data and provides better depth perception and understanding of the operating context. We only need to do a one-time calibration to determine the relation between the HoloLens and the camera. Testing shows that our system achieves high accuracy and low latency. We also show the usefulness of our system in a realistic surgical environment on a cadaveric head. An example of the view directly observed by the surgeon is shown in Figure 1.

Our system takes a step beyond the pioneering research of Cutler et al. [2017] and improves on several aspects. First, our tracking technique does not require significant changes to the shape and weight of the catheter. Second, since we use a stationary camera for tracking, it does not require the user of the HMD to be looking at the catheter to track. This allows the surgeon to freely look anywhere without losing the tracking of the catheter. Finally, the capability of our system is not tied to the HMD. We empirically observed a lag of 1.43 seconds in the video demonstration of Cutler et al. [2017],[2] which is likely caused by the HMD's inability to keep up with the processing. In our system, the images from the camera, as well as the medical volume, are processed separately on another machine, and results are sent to the HMD wirelessly. This allows for faster and more accurate sensing and higher-fidelity medical images. Our system can be naturally integrated with existing medical image registration techniques. A proposed example is illustrated in Figure 1, where the CT slice at the tip of the catheter is displayed if the CT volume is registered with the patient. Due to the scope of this study, we do not perform the medical image registration but refer interested readers to surveys by Kersten-Oertel et al. [2013] and Meola et al. [2016].

[1]See the supplementary video for a demonstration of how commodity depth sensors are unsuitable for catheter tracking.
[2]We observed this at 50 seconds and 51 seconds in the video (https://youtu.be/qqykWW9f41Q).

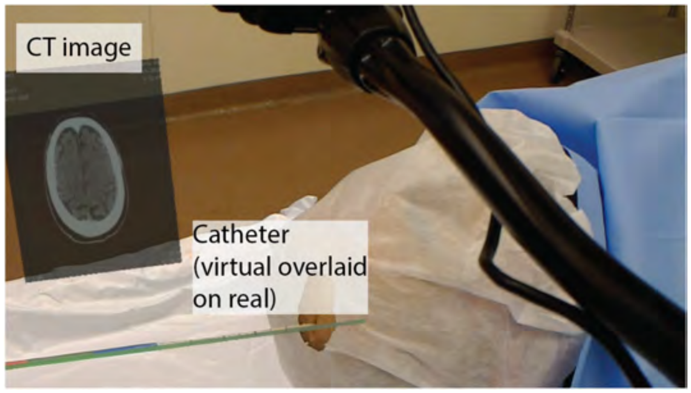

Fig. 1. Results in a realistic surgical scenario where EVD is performed on a cadaveric head. The image was acquired using Microsoft HoloLens with its mixed reality capture functionality and depicts what a surgeon sees when using our system. Additional information could be shown, such as the CT slice at the tip of the catheter if a CT volume is registered to the patient. The CT image shown serves as an illustration of this potential.

In short, we built an AR EVD tracking and visualization system that

- overlays a virtual catheter onto a user's field of view, mimicking the position of the real catheter;
- leaves the catheter functionally unchanged; and
- is accurate and responsive.

The remainder of this article is organized as follows. In Section 2, we cover past research on enhancing surgeon performance in EVD procedures, as well as cases in which AR is used in neurosurgery. In Section 3, we give an overview of our system and introduce how we visualize the catheter based on the result from our algorithm. We cover in detail our algorithm to calculate the position of the catheter in Section 4. In Section 5, we show the stability, accuracy, and latency of our system. Finally, in Section 6, we discuss some limitations of our system, the initial response from medical professionals, and future work.

2 RELATED WORK

EVD has undergone numerous iterations in materials and techniques since it was first performed in the 1740s. The complete documentation of the evolution of EVD is outside the scope of this work; readers can refer to Srinivasan et al. [2014]. In this section, we will review recent developments in EVD catheter placement techniques. In addition, we discuss AR use cases in neurosurgery.

2.1 Catheter Placement

Proper catheter placement is key to the success of an EVD procedure. A 2016 Neurocritical Care Society study [Fried et al. 2016] found that with a stabilization tripod (Ghajar Guide) or other technical adjuncts such as CT guidance, stereotactic navigation could improve accuracy and/or lower the number of EVD procedures performed on a patient.

The Ghajar Guide is a catheterization assistance device in current clinical use, invented by Jamshid Ghajar in 1985. It is a tripod-shaped device that can be securely placed on the patient's skull; the catheter travels along the axis of the device and can be stabilized as it goes into the skull. A study by O'Leary et al. [2000] found that successful catheterization can be achieved either using the Ghajar Guide or freehand, but that a smaller distance to target was achieved with the Ghajar Guide.

For ventricle exploration and catheter placement training, Phillips and John [2000] developed a simple web application that lets trainee surgeons practice simulated catheterization (catheter placement) via a personal computer. Cros et al. [2002] incorporated haptic feedback into the ventriculostomy simulator; users feel a "pop" sensation when the catheter pierces the ventricular surface.

Krombach et al. [2000] conducted free-hand catheterization simulations before performing the actual surgery. In simulations, MRimages were registered onto the patient's head with fiducials. A pointer instrument was tracked by infrared diodes attached to it. The surgeons used the pointer to virtually move the catheter, and the position of the catheter was evaluated.

Luciano et al. [2005] developed the ImmersiveTouch ventriculostomy simulation system. Stereoscopic goggles are tracked electromagnetically and represent the head position. A hand stylus is tracked mechanically and can offer different resistance sensations to simulate the catheter moving in different types of tissue. This way, the displayed content can change according to the user's point of view, and the virtual catheter is visualized based on the location of the hand stylus. Haptic feedback is provided to perceive the interaction between the virtual catheter and the virtual brain model. ImmersiveTouch is used in studies by Banerjee et al. [2007], Lemole et al. [2007], Schirmer et al. [2013], and Yudkowsky et al. [2013].

Tai et al. [2015] 3D printed an actual physical phantom head (manikin head for medical procedure simulations) from the reconstruction of CT images and used the brain model as an EVD training platform. This platform provides a realistic anatomical structure and visual/haptic feedback.

The most recent experimental EVD development is by Li et al. [2018], where the neurosurgeon guides the catheter by aligning it to the displayed trajectory that is shown in an HMD. In an effort to track the catheter, Cutler et al. [2017] attach an optical marker, in this case, a piece of paper, to a rigid catheter. The marker's position, and therefore the catheter's position, is tracked by the camera on an HMD, which displays the virtual catheter image and a 3D model of the damaged part of the brain. This way, as long as the marker is in the camera's field of view, the catheter can be visually tracked, even when the tip is occluded. The system compellingly demonstrates how the advances in sensing and displays can create intuitive and reliable assistance to neurosurgery. Similarly, HoloNeedle of Lin et al. [2018] and the system of Kuzhagaliyev et al. [2018] track the needles for biopsy and ablation with the OptiTrack[3] system and display the virtual needle in an AR headset aligned with the real one. With regard to HoloNeedle [Lin et al. 2018], the biopsy needle's shape is further obtained with embedded Fiber Bragg Grating sensors to take the needle bending into consideration. All systems mentioned previously make a significant change to the shapes of the instruments to accommodate their tracking techniques, which our method avoids (more detail is provided in Section 4). Najafi and Rohling [2011] and Najafi et al. [2015] use a closed-form formula to calculate the trajectory of a needle instrument based on the live footage from a single camera attached to an ultrasound probe and guide the needle angle to reach the target shown in the ultrasound image. Our system is different in that the exact location of the catheter tip is calculated visualized directly in the user's field of view via an AR HMD. Stolka et al. [2014] use stereo cameras to detect the 5DOF information of a needle marked with pseudorandom binary sequence (PRBS) patterns and display the needle in the ultrasound image or project a line on the patient's skin to mimic the needle's location. A generalized version incorporating multiple medical imaging and probing modalities has been proposed by Basafa et al. [2017]. Our system is different in that it uses perspective foreshortening of color bands on the catheter to estimate the tip location from a single camera with higher precision than the prior art.

2.2 AR Interventions for Neurosurgery

One type of AR technique being used in neurosurgery is overlaying detailed preoperative medical image on intraoperative images. Masutani et al. [1998] experimented with overlaying preoperative 3D vascular models onto intraoperative X-ray fluoroscopy images via medical fiducial markers. Two clinical test cases showed the

[3] https://optitrack.com/.

registration reprojection displacement to be below 2.6 mm. Lovo et al. [2007] reconstructed volumes from cerebral MR scans and overlaid the volumes onto intraoperative cerebral images.

One step further is to track the imaging probe (or microscope) during surgery and overlay meaningful information such as anatomy models onto the intraoperative images. Edwards et al. [1995, 2000, 2004] developed and tested an AR microscope-assisted guided intervention system that tracked the microscope and overlaid 3D medical images on the two eyepieces. Shahidi et al. [1998] and Scholz et al. [1998] experimented with similar setups using surgical endoscopes. Kockro et al. [2009] developed a handheld AR system, DEX-Ray, that overlays medical volumes or other images onto a livestream video. Low et al. [2010] used DEX-Ray integrated with the Dextroscope system (an immersive medical image viewing system) and performed meningioma (a type of usually noncancerous brain tumor) excision on five patients. Inoue et al. [2013] tracked off-the-shelf webcams to overlay anatomical medical structures on the webcam images.

Sauer et al. [2001] and Maurer et al. [2001] developed an AR video see-through surgery navigation HMD and demonstrated its use on a phantom head with encouraging results. Two color cameras record the real-world scene, and one additional camera tracks the retroreflective optical markers attached to the phantom head. A medical MR volume aligned with the head phantom is displayed stereoscopically on the HMD. Abe et al. [2013] developed an AR guidance system for percutaneous vertebroplasty, where the insertion location and intended insertion orientation is displayed in an AR HMD. Trials on the phantom show improved accuracy using this system, and successful clinical trials demonstrate practical usability. Abhari et al. [2014] engineered a mixed reality system that facilitates the training and planning for a brain tumor resection procedure and demonstrated the greatly improved performance of junior residents and the reduction in time to perform clinically relevant tasks by clinicians. Li et al. [2018] conducted a clinical EVD trial where manually aligned CT holograms are shown in an AR headset to display the catheter placement trajectory and target location. The catheter is not tracked or visualized, but it took the AR-assisted group fewer passes on average to complete the procedure. The AR-assisted group also had a lower average deviation from the target. Azimi et al. [2018] developed a mixed reality surgical training system that integrates functionalities such as preoperative procedure visualization and real-time performance assessment and demonstrated a catheter placement training session where the system informs the trainee of the orientation error, but the system's tracking accuracy is not reported. Very recently, Meola et al. [2016] and Guha et al. [2017] presented two thorough surveys on the past work in which AR is used for neurosurgery.

3 SYSTEM OVERVIEW

Our system consists of three components: a sensing unit, a processing unit, and a display unit in addition to the modified catheter itself. The functions of each component are described in Section 3.1, as well as the actual hardware used for each component. The way the system is operated in our experiment is described in Section 3.2. Finally, the calibration between the sensing unit and the display unit is described in detail in Section 3.3.

3.1 System Components

The sensing unit captures the live footage of the operation area that contains the modified catheter. The processing unit analyzes the footage and calculates the catheter's position in the camera's reference system (camera space), which is then sent via a wireless network to the display unit. The display unit uses a transformation obtained at the calibration step (more detail is presented in Section 3.3) to transform the received catheter's location into the world reference system (world space) and displays the virtual catheter at that transformed location to overlay the physical catheter. A general illustration of the system, as well as the intended use scenario, can be seen in Figure 2. The workflow of our system is depicted in Figure 3. An actual view captured using HoloLens's mixed reality capture function is shown in Figure 1.

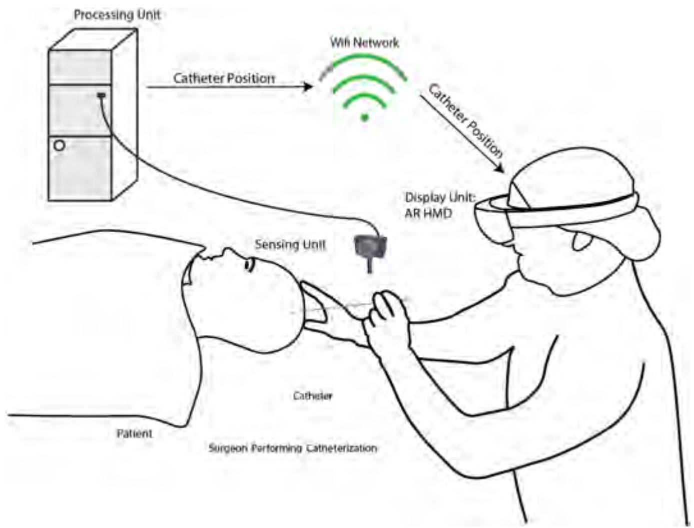

Fig. 2. System overview.

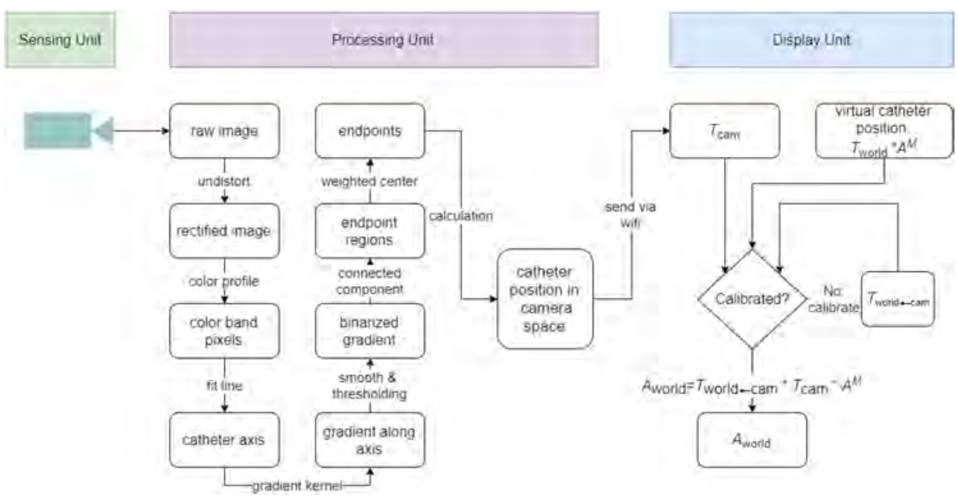

Fig. 3. Workflow of the system.

The sensing unit is an off-the-shelf Logitech c920 web camera on a tripod. The reason we use a separate camera, rather than the one integrated into the display, is to avoid being limited by the quality of the integrated camera and the processing capabilities of the display, as well as reduce network latency. The processing unit is an Alienware laptop computer with an Intel i7 7820HK processor running at 2.9 GHz. The display unit is a Microsoft HoloLens tetherless AR HMD.

The catheter used in our experiment is a Codman EDS 3 clear ventricular CSF catheter. This catheter measures 35 cm in length, which is typical of catheters used in EVD. Fried et al. [2016] suggest that, in surgical scenarios, the catheter should not penetrate the skull by more than 6.5 cm, and therefore we place the color bands 7 cm away from the tip. We use three color bands, each 3.8 cm in length (see Figure 5 for an illustration).

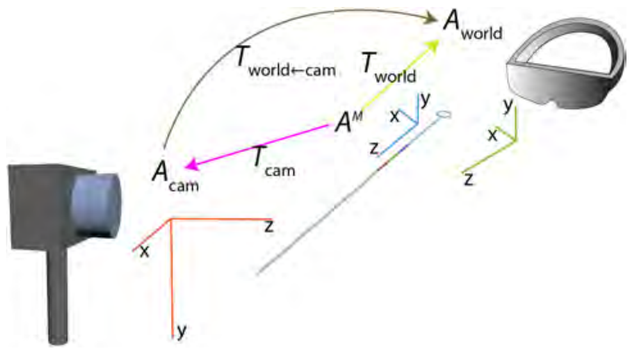

Fig. 4. Reference system mapping.

3.2 System Operation

When using this system, the user wears the HMD, which displays a virtual catheter. The virtual catheter can be dragged around in the world space with hand gestures. After the user manually aligns the virtual catheter with the physical one observed through the HMD, the user issues a calibration command that triggers the system to calculate the mapping from the camera space to the world space. The system then uses this mapping to transform the catheter's location in the camera space into the world space as mentioned previously for the subsequent frames, until a new calibration command is issued when the users see fit.

In the experiment, the surgeons held the rear portion of the catheter as illustrated in Figure 2 to avoid occluding the color bands.

3.3 Reference System Mapping

Our algorithm calculates the position of the catheter in the camera space. To be able to visualize the catheter in the HMD, a way to transform from the camera space to the world space is required. We achieve this by doing a one-time calibration with the calculated catheter position in the camera space and the virtual catheter position in the world space. Suppose the coordinate of the catheter in its own reference system (model space) is A^M. At a certain frame, T_{cam} and T_{world} transform A^M into the camera space ($A_{cam} = T_{cam}A^M$) and the world space ($A_{world} = T_{world}A^M$), respectively. We want to find a transformation $T_{world \leftarrow cam}$ that will transform from the camera space to the world space.

$$T_{world \leftarrow cam} T_{cam} A^M = T_{world} A^M \tag{1}$$

For this to work with every A^M, we simply take the following.

$$T_{world \leftarrow cam} = T_{world} T_{cam}^{-1} \tag{2}$$

Then with every frame where a new T_{cam} is calculated from the position of the catheter in the image, we can calculate the corresponding T_{world} and display the virtual catheter. Reference system mapping is illustrated in Figure 4.

4 CATHETER TRACKING

We present a novel method of tracking the 3D position of the catheter in real time, enabled by three color bands painted on the catheter. The three color bands are adjacent, and we know each of their lengths and locations relative to the catheter; the colors only need to be sufficiently distinct to be identified in the image (Figure 5).

We use a pinhole model to represent the camera. As seen in Figure 6, P is the center of projection of the pinhole model and is the origin point in the camera space. We observe in the image the 2D coordinates of the catheter A', B', and C' (Figure 6 shows three endpoints of two color bands as an example). Given that we know the lengths

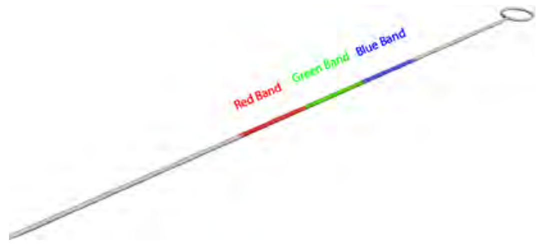

Fig. 5. Drawing of the catheter and the color bands. The color bands need to be distinct and adjacent. The lengths of the three color bands, as well as the uncolored forward portion (from the catheter tip to the beginning of the first color band) of the catheter, are known. With the lengths and the positions of the color band endpoints detected in the camera space, we can calculate the 5DOF (no roll) information of the catheter and infer the position of the tip.

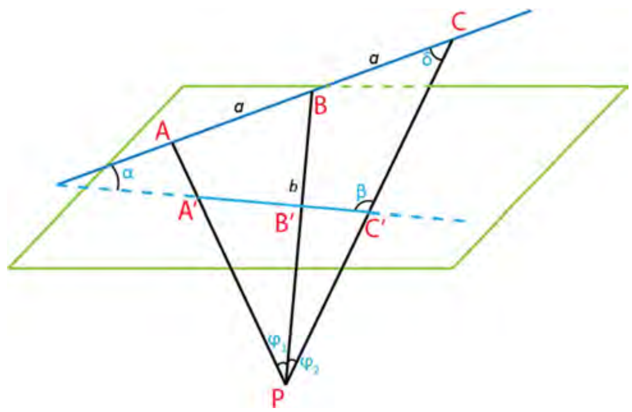

Fig. 6. We need to find the angle α between the catheter and its image. Let A, B, and C be three endpoints of two consecutive color bands. The color bands are of equal length a. P is the center of projection in the pinhole camera model. The distance between B and P is b.

of the color bands $|AB|$ and $|BC|$, this becomes a simplified version of the perspective three-point problem (P3P) thoroughly studied and documented in other works [Ameller et al. 2000; Gao et al. 2003; Marchand et al. 2016; Quan and Lan 1999]. In a general P3P problem, there could be as many as four solutions. In our case, where the three points are collinear, there could be two solutions, of which only one is desired. Determining the correct solution requires finding the angle between the catheter and its image in the image plane, shown in Figure 6.

We describe our approach to the P3P problem in the following. First, we use a geometric method to find α in Section 4.1. Then, we calculate the position of the catheter in Section 4.2. Finally, we extract the segments' endpoints A', B', and C' from the image in Section 4.3.

4.1 Angle α

We denote the three endpoints of two consecutive color bands as A, B, and C in Figure 6, and the center of projection as P. The images of A, B, and C are A', B', and C' on the image plane. Given the camera intrinsics that can be obtained by a one-time calibration, we can explicitly represent P, A', B', and C' with exact coordinates in pixels. We can calculate the angles as follows.

$$\angle APB = \varphi_1 = \operatorname{acos} \frac{\mathbf{PA'} \cdot \mathbf{PB'}}{|\mathbf{PA'}||\mathbf{PB'}|} \tag{3}$$

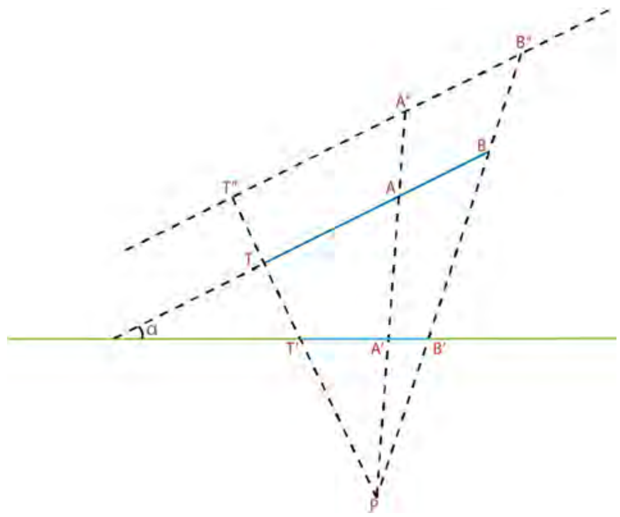

Fig. 7. Finding the position of the catheter in the camera space. P is the center of projection. TA is the uncolored forward portion of the catheter. AB is the first color band on the catheter.

$$\angle BPC = \varphi_2 = \operatorname{acos}\frac{\mathbf{PB'} \cdot \mathbf{PC'}}{|\mathbf{PB'}||\mathbf{PC'}|} \tag{4}$$

Now assume the two color segments are of equal length a (assume $|AB| = |BC| = a$) and $|PB| = b$. Trigonometric equations give the following.

$$\frac{a}{\sin\varphi_1} = \frac{b}{\sin(\pi - \varphi_1 - \varphi_2 - \delta)} \tag{5}$$

$$\frac{a}{\sin\varphi_2} = \frac{b}{\sin\delta} \tag{6}$$

δ is the angle $\angle ACP$. Solving for δ,

$$\delta = \operatorname{atan}\left(\frac{\sin\varphi_2 \sin(\varphi_1 + \varphi_2)}{(\sin\varphi_1 - \sin\varphi_2 \cos(\varphi_1 + \varphi_2))}\right). \tag{7}$$

Then we can calculate $\alpha = \pi - \beta - \delta$. α could be either positive or negative depending on whether A is farther away from the image plane than C or closer. When A is closer than C (see Figure 6), $\alpha > 0$. When A is farther, $\alpha < 0$.

4.2 Position of Catheter

With the 3D orientation, we can calculate the position of the catheter in the camera space. In Figure 7, AB represents a color band. AT represents the portion of the catheter from the tip to the color band. AT may not be entirely visible from the camera. A', B', and T' are the images of A, B, and T on the image plane, respectively. We know the lengths of $\boldsymbol{A'B'}$ because we have detected them in the image. We know the lengths of $\boldsymbol{PA'}$ and $\boldsymbol{PB'}$ as well.

The actual catheter is in the plane formed by P and $T'B'$, and we know its orientation. But it could be on any line that is parallel to TB—for example, $T''B''$. We can set $\boldsymbol{PA''} = m\boldsymbol{PA'}$. The actual ratio m does not really matter because a different ratio only leads to a parallel line to BC. We can assume, for example, $m = 10$, and let $\boldsymbol{PB''} = k\boldsymbol{PB'}$. Then $\boldsymbol{A''B''} = \boldsymbol{PB''} - \boldsymbol{PA''} = k\boldsymbol{PB'} - \boldsymbol{PA''}$.

We know the angle formed by the catheter and its image α, which is the angle formed by $A''B''$ and $A'B'$.

$$\boldsymbol{A''B''} \cdot \boldsymbol{A'B'} = |\boldsymbol{A''B''}||\boldsymbol{A'B'}|\cos\alpha \tag{8}$$

Equation (8) can be further transformed into

$$k\boldsymbol{PB'} \cdot \boldsymbol{A'B'} - \boldsymbol{PA''} \cdot \boldsymbol{A'B'} = \sqrt{k^2\boldsymbol{PB'}^2 - 2k\boldsymbol{PB'}\boldsymbol{PA''} + \boldsymbol{PA''}^2}|\boldsymbol{A'B'}|\cos\alpha. \tag{9}$$

All values in Equation (9) are known except for k. We can solve k and thus find the position of B''. It is worth noting that Equation (9) is a quadratic equation, and there could be two solutions for k. Judging from Figure 7, if $\alpha > 0$, B should be farther away from the image plane than A. Therefore, k should be greater than the assumed ratio of $|\boldsymbol{PA''}|$ over $|\boldsymbol{PA'}|$ and vice versa.

Now that we know the length of the catheter color band AB in the real world, we can calculate the position of the color band AB in the camera space.

$$\boldsymbol{PA} = \frac{|\boldsymbol{AB}|}{|\boldsymbol{A''B''}|}\boldsymbol{PA''} \tag{10}$$

$$\boldsymbol{PB} = \frac{|\boldsymbol{PA}|}{|\boldsymbol{PA''}|}\boldsymbol{PB''} \tag{11}$$

Since we know where AB is on the catheter, we can calculate the position of the catheter in the camera space. For example, from

$$\boldsymbol{PT} = \boldsymbol{PA} - \frac{|\boldsymbol{AB}|}{|\boldsymbol{AT}|}\boldsymbol{AB}, \tag{12}$$

we can calculate the position of the tip in the camera space since we know the lengths of the uncolored forward portion of the catheter and the color bands.

It is worth noting that we can calculate the position of the catheter with two adjacent color bands. We use three color bands to make our system robust against occlusion and improve accuracy when all three are visible.

4.3 Color Band Detection

In the color band detection step, the input is an image I of the catheter (P_{catheter} being all pixels that belong to the catheter), and the output is the locations of the endpoints of the color bands. The accuracy of the color band detection is the most important factor in finding the catheter tip. To reliably detect the endpoints of the color bands, we develop a new algorithm (see Figure 3). Starting from the original image (Figure 8(a)) and its undistorted result (Figure 8(b)), we first use simple thresholds to get the most of the pixels $P^*_{\text{catheter}} \subseteq P_{\text{catheter}}$ of the catheter in the image. We then fit these pixels to a line, which we refer to as the axis L_{axis} of the catheter (Figure 8(c)). The gradient $G_{L_{\text{axis}}}$ along the direction of L_{axis} is calculated using a variation of Sobel filter $K_{L_{\text{axis}}}$ that is weighed anisotropically according to L_{axis} (Figure 8(d)). $G_{L_{\text{axis}}}$ has high values near the border of two different colors. After smoothing using a median filter, the gradient map is thresholded into binary images $G^*_{L_{\text{axis}}}$ with positive values where the borders are (Figure 8(e)). Finally, we take the weighted centers of the connected components of $G^*_{L_{\text{axis}}}$ as the endpoints of color bands (Figure 8(f)). Our processing technique is robust against blurry images caused by motion, as seen in Figure 8(g–i).

5 ACCURACY ANALYSIS

In this section, we analyze the performance of our proposed algorithm. First, we measure the stability of our tracking algorithm. Then, we test tracking accuracy on a 2D planar grid and a specially designed and 3D-printed grid. Finally, we test the latency compared with a third-party tracker.

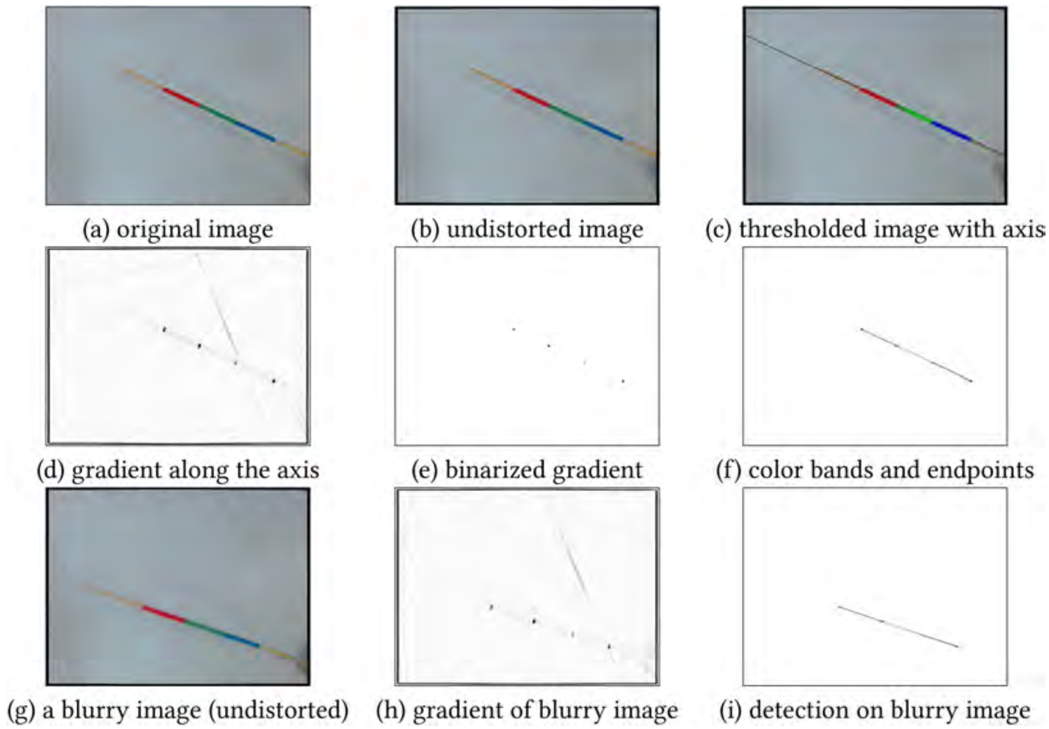

Fig. 8. Detecting endpoints. Parts (g) through (i) show detecting endpoints in an image where the catheter is blurry because of movement. Our algorithm is able to handle this case.

5.1 Stability

Given the color segment endpoints detected in the image, our tracking algorithm will output the computed catheter position. The instability in the tracking algorithm comes from random noise in each frame. The noise could cause the same endpoint in two frames to be detected a few pixels apart, even when the catheter stays still.

We measure the stability as the root mean square of the change of calculated tip in the camera space in two consecutive frames as in Niehorster et al. [2017] while keeping the catheter still. Given n frames, and the tip of the catheter in frame i as $\boldsymbol{x_i}$, the stability is measured as follows.

$$S_{RMS} = \sqrt{\frac{1}{n-1}\sum_{i=1}^{n-1} ||\boldsymbol{x_i} - \boldsymbol{x_{i+1}}||^2} \tag{13}$$

Several factors could influence the stability of the tracking algorithm, including lighting condition, thresholds for color segmentation, and distance from the camera to the catheter. In a typical laboratory setting, our algorithm achieves a stability of 0.33 mm as measured over 870 frames.

5.2 Accuracy over a 2D Grid

To test the accuracy of the tracking algorithm, we move and point the tip of the catheter at the intersections of a grid. The grid, which is 8.16 × 8.16 cm in size, is printed on a white sheet. This provides enough space to test the accuracy of catheter movement, more than the 6.5 cm suggested by Fried et al. [2016]. The setup for this test can be seen in Figure 9(a).

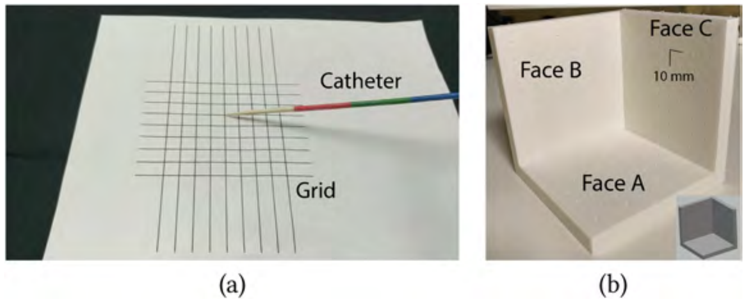

Fig. 9. Setup for testing the tracking accuracy over a 2D grid (a) and tracking accuracy over a 3D grid with the 3D CAD model in the lower right (b).

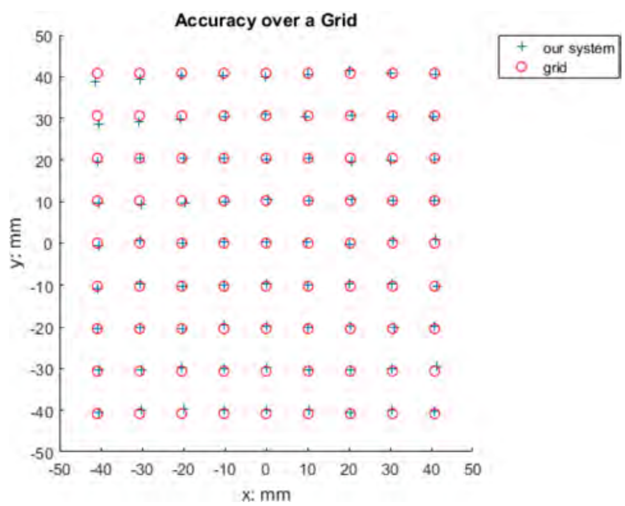

Fig. 10. Accuracy of our catheter tracking approach over the 2D grid. The red circles indicate the grid intersection. The blue crosses indicate the computed catheter tip position.

We assume the center intersection of the grid to be a reference point. Before the test, a 2D marker is placed on the workbench, and its up and right directions (parallel to the edges of the paper sheet on which the marker is printed) in the camera space are detected. The sheet with the grid is then placed on top of the marker with the edges aligned. Therefore, the grid has the same up and right direction as the marker, and with its size known, we know the position of each grid intersection relative to the reference point. When moving along the grid, the catheter's orientation is kept relatively fixed and its tip position in the camera space is recorded. Then the tip positions relative to that when the tip is pointed at the reference point is compared to positions of the grid intersections relative to the reference point.

Figure 10 shows the catheter tip locations on the grid with the reference point as the origin. Blue circles indicate the grid intersections, and the orange crosses are the detected catheter tips. The average distance from the catheter tip to the corresponding grid intersections is 0.58 mm.

5.3 Accuracy over a 3D Grid

We also demonstrate the accuracy of our algorithm when the catheter is moving in vertical space. To construct a reliable ground truth, we use a 3D-printed structure where square grids of blind holes are on its three faces

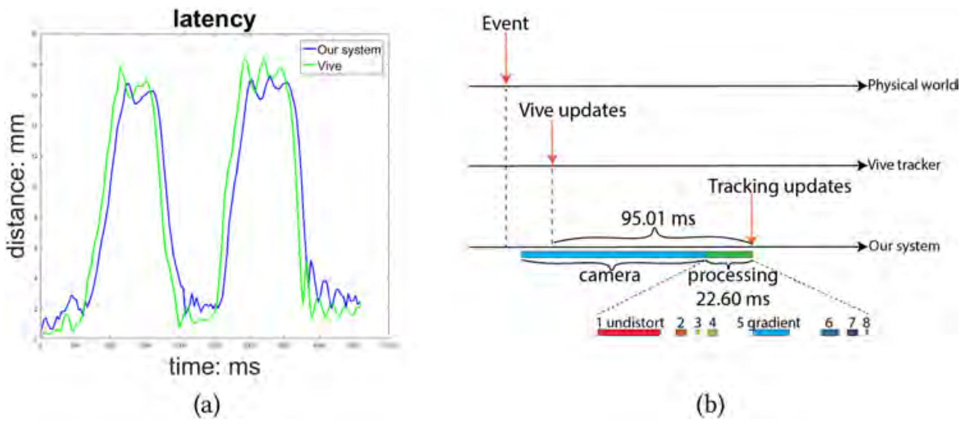

Fig. 11. Latency of our system compared to an HTC Vive tracker (a) and the various components of our system's latency in image capture and processing (b).

(see Figure 9). The centers of the blind holes are $d = 10$ mm apart in both directions, which we manually verified with a caliper. Each blind hole is designed to be a cone with 1 mm radius and 3 mm height. On each face, there are 8×8 blind holes.

When testing on each face, one of the center blind holes (e.g., (m, n) on the 8×8 grid) is chosen as the reference point. The location of the tip when the needle tip is inserted into each blind hole (i, j) is recorded as $T(i, j)$. We construct the ground truth $G(i, j)$ as the designed distance of each blind hole to the reference point $G(i, j) = \sqrt{(m-i)^2 + (n-j)^2}d$. The distance between the calculated tip and the reference at each blind hole is $D(i, j) = ||T(i, j) - T(m, n)||_2$. The average accuracy on the face f is then $\text{Acc}_f = \frac{1}{64}\sum_{i,j}|G(i, j) - D(i, j)|$.

In this test, $\text{Acc}_A = 0.49$ mm, $\text{Acc}_B = 0.93$ mm, and $\text{Acc}_C = 1.12$ mm. The overall average accuracy on all three faces is 0.85 mm.

5.4 Latency

We measure our tracking system's latency using an HTC Vive tracker, which according to Niehorster et al. [2017] itself has a 22-ms latency. This latency is measured as the time elapsed between the tracker update and our system catheter's location update. In our test, we rapidly move the catheter, which is attached to the tracker, and record for each frame the distance from the catheter tip (tracked with our system and by the HTC Vive tracker) to their original location recorded at the beginning of the test. The distances are then plotted, and we manually measure average time by which our system lags the tracker. Figure 11(a) shows the plotted distances that we recorded. Manual measurements show an average latency of 95.01 ms. A breakdown of the latency can be seen in Figure 11(b).

There are two factors in the latency with respect to the HTC Vive tracker. It takes about 72 ms for our camera (together with the driver and OpenCV functions) to capture and store the image. The processing takes an additional 22.60 ms on our machine, which uses an Intel i7 7820HK processor running at 2.9 GHz. As we show in Table 1, undistorting takes the longest time (10.05 ms per frame, 44.42% of the total processing time). Speedup may be achieved by performing color segmentation first and undistorting only the pixels of the color bands. The next most time consuming task is calculating the gradient along the catheter axis (6.81 ms per frame, 30.12% of total processing time). Our current implementation is on the CPU. A GPU is likely to reduce the processing time through parallelization. A professional-grade camera with a low image capture time can greatly reduce the latency.

Table 1. Time Breakdown of Functions in Tracking

ID	Function	Avg. Time per Frame (ms)	Percentage in Processing (%)
1	Undistort	10.04	44.42
2	Color segmentation	1.05	4.64
3	Erosion	0.23	1.02
4	Get axis	0.93	4.13
5	Gradient	6.81	30.12
6	Connected components	1.15	5.08
7	Weighted centroids	0.92	4.09
8	Calculate catheter position	0.21	0.92
	Other	1.26	5.58
	Total	22.60	100.00

6 DISCUSSION AND FUTURE WORK

We have demonstrated a novel method of tracking a catheter and projecting it onto an AR display. Better visualization during EVD placement has the potential to make a risky procedure safer and save lives. In combination with CT scan projection of the skull, this could potentially provide the neurosurgeons with a clear view of where the catheter is relative to the insertion target inside the skull of a patient. We address the challenges of significantly enhancing the accuracy and latency of our system over the state-of-the-art AR systems for this procedure, such as that of Cutler et al. [2017].

EVD is a technically difficult procedure. It involves placing a catheter several centimeters into the brain through tissues of varying density, including bone, dura, brain, and cerebrospinal fluid. In addition, it is generally performed in bright light with blue sterile drapes. These realities can potentially affect the accuracy of AR tip projection in difficult-to-predict ways and needed to be validated in our study. Furthermore, the AR system should not interfere with procedure performance by not hindering the surgeon placing the drain. A purely computational evaluation of our approach would not have been sufficient to assess the efficacy of our AR approach in such challenging environments.

To validate the true feasibility of AR-assisted EVD placement, we carried out our evaluation in a realistic experimental environment, which included a cadaveric head, using sterile drapes and the existing EVD placement kits, closely mimicking actual EVD placement in a patient. After inserting the catheter tip at the insertion point, the surgeons advanced the catheter in a straight line. During the process, the displayed virtual catheter projection aligned well with the visible portion of the real catheter, and the pace at which the real and the virtual catheter moved matched. The surgeons reported that the handling of our slightly modified catheter feels identical to a traditional catheter, and although aware of the HMD, they did not find it cumbersome. An image of a surgeon using our system in the experiment can be seen in Figure 12.

Tests show that our tracking method is accurate with submillimeter accuracy and low latency. If further improvements in accuracy and latency were needed, we could do so with the following enhancements. First, a professional-grade camera with a higher resolution, higher dynamic range, and lower latency could improve tracking by enhancing our ability to discern the segment endpoints and reduce the overall latency. With a higher resolution, the camera could be farther away from the catheter without compromising tracking quality, thus allowing a larger tracking area. All of this comes with a higher computational burden. At the moment, our algorithm is implemented on a CPU but is highly parallelizable. Implementing a parallel GPU version of the algorithm is a high priority in our future work. At present, we observe around 167-ms end-to-end latency between moving the real catheter and its updating the virtual catheter in the HMD. In our current system, we use an independent camera and a laptop for processing, but it would be desirable to explore an all-in-one setup. This is highly likely with further advances in commodity HMDs. Current-generation AR HMDs often suffer

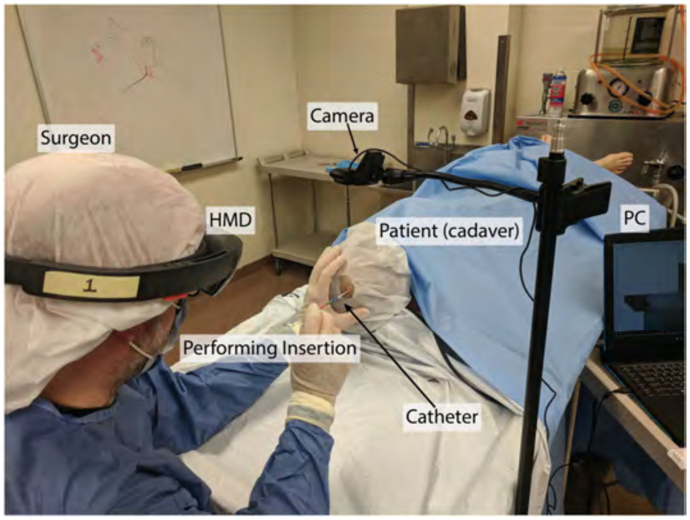

Fig. 12. Our system being used in a cadaver study.

from drift in spatial tracking. In our studies, this has ranged from 2.15 to 6.35 mm, depending on the amount of user head movement. Complementing the 3D spatial tracking with 2D optical tracking as in Frantz et al. [2018] should be able to improve spatial tracking accuracy.

In our system, the calibration between the camera space and the world space is performed manually to make sure the observed virtual catheter aligns with the observed physical catheter. Therefore, very little optical misalignment has been observed in our experiment as long as the user does not remove or adjust how the HMD is worn. We believe that this limitation shall be largely addressed by eye tracking and better optical alignment in the next-generation HMDs. As the next-generation HMDs support a higher resolution and a wider field of view, it should be possible to further support the presentation of time-critical information to assist in procedures such as EVD. This information could be presented in both peripheral regions [Sun and Varshney 2018] and foveal regions [Meng et al. 2018] of the surgeon's field of view.

Most catheters used in EVD (e.g., Integra, Medtronic, and Codman) measure longer than 30 cm and there is sufficient space to include color bands, as outlined in our approach, on clinical catheters. To further mitigate occlusion-related concerns around color bands, one could explore adding additional redundant color bands. Last but not least, attention needs to be paid to the clinical safety of catheter modification. Technologies such as VisiMark[4] could be used to create medical-grade markings to serve as the color bands. Alternatively, the catheter could be constructed with medical-grade silicone of various colors and go through standard sterilization. Slight changes would need to be made to the color band detection process.

7 CONCLUSION

We present an AR surgical visualization and tracking system that can assist surgeons in EVD catheter placement. Compared to existing similarly purposed systems, our system does not require changing the shape or weight of the medical instruments. Our main technical contributions include (1) a low-latency, high-performance way to track catheters and other 5DOF thin cylindrical objects, and (2) an image processing algorithm to extract tracking color segment endpoints in an image. Tests show that our tracking method achieves a 0.58-mm accuracy on a 2D plane and an accuracy of 0.85 mm in 3D space. Processing for each frame takes 22.60 ms on a moderately

[4] http://www.surfacesolutionsgroup.com/coatings/visi-mark/.

powerful computer. Both the accuracy and speed can be further improved with higher-quality cameras and parallel implementation. We tested our system in a realistic surgical environment with a cadaveric head. Our color marker and tracking technique can be applied to other medical procedures where the precise location of a very thin medical instrument is needed, such as needle-guided biopsies and minimally invasive surgeries.

ACKNOWLEDGMENTS

We sincerely appreciate the anonymous reviewers for their insightful and exceptionally thorough reviews that have greatly helped us in improving this paper. We would also like to thank Barbara Brawn-Cinani for her constructive advice and comments that were vital to refining our presentation and Jonathan Heagerty for his help with designing and fabricating the necessary tools for testing our system.

REFERENCES

Yuichiro Abe, Shigenobu Sato, Koji Kato, Takahiko Hyakumachi, Yasushi Yanagibashi, Manabu Ito, and Kuniyoshi Abumi. 2013. A novel 3D guidance system using augmented reality for percutaneous vertebroplasty. *Journal of Neurosurgery: Spine* 19, 4 (2013), 492–501.

Kamyar Abhari, John S. H. Baxter, Elvis C. S. Chen, Ali R. Khan, Terry M. Peters, Sandrine de Ribaupierre, and Roy Eagleson. 2014. Training for planning tumour resection: Augmented reality and human factors. *IEEE Transactions on Biomedical Engineering* 62, 6 (2014), 1466–1477.

Marc-André Ameller, Bill Triggs, and Long Quan. 2000. Camera pose revisited: New linear algorithms. https://hal.inria.fr/inria-00548306.

Ehsan Azimi, Camilo Molina, Alexander Chang, Judy Huang, Chien-Ming Huang, and Peter Kazanzides. 2018. Interactive training and operation ecosystem for surgical tasks in mixed reality. In *OR 2.0 Context-Aware Operating Theaters, Computer Assisted Robotic Endoscopy, Clinical Image-Based Procedures, and Skin Image Analysis*. Springer, 20–29.

P. Pat Banerjee, Cristian J. Luciano, G. Michael Lemole Jr., Fady T. Charbel, and Michael Y. Oh. 2007. Accuracy of ventriculostomy catheter placement using a head-and hand-tracked high-resolution virtual reality simulator with haptic feedback. *Journal of Neurosurgery* 107, 3 (2007), 515–521.

Ehsan Basafa, Pezhman Foroughi, Martin Hossbach, Jasmine Bhanushali, and Philipp Stolka. 2017. Visual tracking for multi-modality computer-assisted image guidance. In *Medical Imaging 2017: Image-Guided Procedures, Robotic Interventions, and Modeling*, Vol. 10135. International Society for Optics and Photonics, Bellingham, WA, 101352S.

Olivier Cros, Morten Volden, Jens Jørgen Flaaris, Lars Chebørløv Brix, Christian Fischer Pedersen, Kim Vang Hansen, Ole Vilhelm Larsen, Lasse Riis Østergaard, and Jens Haase. 2002. Simulating the puncture of the human ventricle. In *Proceedings of the 10th Annual Medicine Meets Virtual Reality Conference*.

Andrew Benjamin Cutler, Shervin Rahimpour, Yameng Liu, Nandan Lad, Regis Kopper, and Patrick Codd. 2017. Development of augmented reality-based neuro-navigation system for use in external ventricular drain placement. *Journal of Neurosurgery* . 126 (2017), A1438. https://youtu.be/qqykWW9f41Q.

Ruofei Du, Ming Chuang, Wayne Chang, Hugues Hoppe, and Amitabh Varshney. 2019. Montage4D: Real-time seamless fusion and stylization of multiview video textures. *Journal of Computer Graphics Techniques* 8, 1 (Jan. 2019), 1–34. DOI: https://doi.org/10.1145/3190834.3190843

Philip J. Edwards, Derek L. G. Hill, David J. Hawkes, R. Spink, Alan C. F. Colchester, A. Strong, and M. Gleeson. 1995. Neurosurgical guidance using the stereo microscope. In *Computer Vision, Virtual Reality and Robotics in Medicine*. Springer, 555–564.

Philip J. Edwards, Laura G. Johnson, David J. Hawkes, Michael R. Fenlon, Anthony J. Strong, and Michael J. Gleeson. 2004. Clinical experience and perception in stereo augmented reality surgical navigation. In *Proceedings of the International Workshop on Medical Imaging and Virtual Reality*. Springer, 369–376.

P. J. Edwards, A. P. King, C. R. Maurer, D. A. De Cunha, D. J. Hawkes, D. L. G. Hill, R. P. Gaston, et al. 2000. Design and evaluation of a system for microscope-assisted guided interventions (MAGI). *IEEE Transactions on Medical Imaging* 19, 11 (2000), 1082–1093.

Zhencheng Fan, Guowen Chen, Junchen Wang, and Hongen Liao. 2017. Spatial position measurement system for surgical navigation using 3-D image marker-based tracking tools with compact volume. *IEEE Transactions on Biomedical Engineering* 65, 2 (2017), 378–389.

Taylor Frantz, Bart Jansen, Johnny Duerinck, and Jef Vandemeulebroucke. 2018. Augmenting Microsoft's HoloLens with vuforia tracking for neuronavigation. *Healthcare Technology Letters* 5, 5 (2018), 221–225.

Herbert I. Fried, Barnett R. Nathan, A. Shaun Rowe, Joseph M. Zabramski, Norberto Andaluz, Adarsh Bhimraj, Mary McKenna Guanci, David B. Seder, and Jeffrey M. Singh. 2016. The insertion and management of external ventricular drains: An evidence-based consensus statement. *Neurocritical Care* 24, 1 (2016), 61–81.

Xiao-Shan Gao, Xiao-Rong Hou, Jianliang Tang, and Hang-Fei Cheng. 2003. Complete solution classification for the perspective-three-point problem. *IEEE Transactions on Pattern Analysis and Machine Intelligence* 25, 8 (2003), 930–943.

Daipayan Guha, Naif M. Alotaibi, Nhu Nguyen, Shaurya Gupta, Christopher McFaul, and Victor X. D. Yang. 2017. Augmented reality in neurosurgery: A review of current concepts and emerging applications. *Canadian Journal of Neurological Sciences* 44, 3 (2017), 235–245.

David R. Huyette, Benjamin J. Turnbow, Christian Kaufman, Dale F. Vaslow, Benjamin B. Whiting, and Michael Y. Oh. 2008. Accuracy of the freehand pass technique for ventriculostomy catheter placement: Retrospective assessment using computed tomography scans. *Journal of Neurosurgery* 108, 1 (2008), 88–91.

D. Inoue, B. Cho, M. Mori, Y. Kikkawa, T. Amano, A. Nakamizo, K. Yoshimoto, et al. 2013. Preliminary study on the clinical application of augmented reality neuronavigation. *Journal of Neurological Surgery Part A: Central European Neurosurgery* 74, 02 (2013), 071–076.

Udaya K. Kakarla, Louis J. Kim, Steven W. Chang, Nicholas Theodore, and Robert F. Spetzler. 2008. Safety and accuracy of bedside external ventricular drain placement. *Operative Neurosurgery* 63, suppl._1 (2008), ONS162–ONS167.

Marta Kersten-Oertel, Pierre Jannin, and D. Louis Collins. 2013. The state of the art of visualization in mixed reality image guided surgery. *Computerized Medical Imaging and Graphics* 37, 2 (2013), 98–112.

Ralf A. Kockro, Yeo Tseng Tsai, Ivan Ng, Peter Hwang, Chuangui Zhu, Kusuma Agusanto, Liang Xiao Hong, and Luis Serra. 2009. DEX-Ray: Augmented reality neurosurgical navigation with a handheld video probe. *Neurosurgery* 65, 4 (2009), 795–808.

G. Krombach, A. Ganser, Ch Fricke, V. Rohde, M. Reinges, J. Gilsbach, and U. Spetzger. 2000. Virtual placement of frontal ventricular catheters using frameless neuronavigation: An “unbloody training” for young neurosurgeons. *Minimally Invasive Neurosurgery* 43, 04 (2000), 171–175.

Timur Kuzhagaliyev, Neil T. Clancy, Mirek Janatka, Kevin Tchaka, Francisco Vasconcelos, Matthew J. Clarkson, Kurinchi Gurusamy, David J. Hawkes, Brian Davidson, and Danail Stoyanov. 2018. Augmented reality needle ablation guidance tool for irreversible electroporation in the pancreas. In *Medical Imaging 2018: Image-Guided Procedures, Robotic Interventions, and Modeling*, Vol. 10576. International Society for Optics and Photonics, Bellingham, WA, 1057613.

G. Michael Lemole Jr., P. Pat Banerjee, Cristian Luciano, Sergey Neckrysh, and Fady T. Charbel. 2007. Virtual reality in neurosurgical education: Part-task ventriculostomy simulation with dynamic visual and haptic feedback. *Neurosurgery* 61, 1 (2007), 142–149.

Ye Li, Xiaolei Chen, Ning Wang, Wenyao Zhang, Dawei Li, Lei Zhang, Xin Qu, et al. 2018. A wearable mixed-reality holographic computer for guiding external ventricular drain insertion at the bedside. *Journal of Neurosurgery* 1, AOP (2018), 1–8.

M. A. Lin, A. F. Siu, J. H. Bae, M. R. Cutkosky, and B. L. Daniel. 2018. HoloNeedle: Augmented reality guidance system for needle placement investigating the advantages of three-dimensional needle shape reconstruction. *IEEE Robotics and Automation Letters* 3, 4 (Oct. 2018), 4156–4162. DOI: https://doi.org/10.1109/LRA.2018.2863381

Eduardo E. Lovo, Juan C. Quintana, Manuel C. Puebla, Gonzalo Torrealba, José L. Santos, Isidro H. Lira, and Patricio Tagle. 2007. A novel, inexpensive method of image coregistration for applications in image-guided surgery using augmented reality. *Operative Neurosurgery* 60, suppl._4 (2007), ONS–366.

David Low, Cheng Kiang Lee, Lee Lian Tay Dip, Wai Hoe Ng, Beng Ti Ang, and Ivan Ng. 2010. Augmented reality neurosurgical planning and navigation for surgical excision of parasagittal, falcine and convexity meningiomas. *British Journal of Neurosurgery* 24, 1 (2010), 69–74.

Cristian Luciano, Pat Banerjee, G. Michael Lemole, and Fady Charbel. 2005. Second generation haptic ventriculostomy simulator using the ImmersiveTouch system. *Studies in Health Technology and Informatics* 119 (2005), 343.

Eric Marchand, Hideaki Uchiyama, and Fabien Spindler. 2016. Pose estimation for augmented reality: A hands-on survey. *IEEE Transactions on Visualization and Computer Graphics* 22, 12 (2016), 2633–2651.

Yoshitaka Masutani, Takeyoshi Dohi, Fumitaka Yamane, Hiroshi Iseki, and Kintomo Takakura. 1998. Augmented reality visualization system for intravascular neurosurgery. *Computer Aided Surgery* 3, 5 (1998), 239–247.

Calvin R. Maurer Jr., Frank Sauer, Bo Hu, Benedicte Bascle, Bernhard Geiger, Fabian Wenzel, Filippo Recchi, et al. 2001. Augmented reality visualization of brain structures with stereo and kinetic depth cues: System description and initial evaluation with head phantom. *Medical Imaging* 2001 (2001), 445–456.

Xiaoxu Meng, Ruofei Du, Matthias Zwicker, and Amitabh Varshney. 2018. Kernel foveated rendering. *Proceedings of the ACM on Computer Graphics and Interactive Techniques* 1, 1, (May 2018), Article 5, 20 pages. DOI: https://doi.org/10.1145/3203199

Antonio Meola, Fabrizio Cutolo, Marina Carbone, Federico Cagnazzo, Mauro Ferrari, and Vincenzo Ferrari. 2016. Augmented reality in neurosurgery: A systematic review. *Neurosurgical Review* 40, 4 (2016), 537–548.

Mohammad Najafi, Purang Abolmaesumi, and Robert Rohling. 2015. Single-camera closed-form real-time needle tracking for ultrasound-guided needle insertion. *Ultrasound in Medicine & Biology* 41, 10 (2015), 2663–2676.

Mohammad Najafi and Robert Rohling. 2011. Single camera closed-form real-time needle trajectory tracking for ultrasound. In *Medical Imaging 2011: Visualization, Image-Guided Procedures, and Modeling*, Vol. 7964. International Society for Optics and Photonics, Bellingham, WA, 79641F.

Diederick C. Niehorster, Li Li, and Markus Lappe. 2017. The accuracy and precision of position and orientation tracking in the HTC Vive virtual reality system for scientific research. *i-Perception* 8, 3 (2017), 177–205.

Shaun T. O’Leary, Max K. Kole, Devon A. Hoover, Steven E. Hysell, Ajith Thomas, and Christopher I. Shaffrey. 2000. Efficacy of the Ghajar Guide revisited: A prospective study. *Journal of Neurosurgery* 92, 5 (2000), 801–803.

Nicholas I. Phillips and Nigel W. John. 2000. Web-based surgical simulation for ventricular catheterization. *Neurosurgery* 46, 4 (2000), 933–937.

Long Quan and Zhongdan Lan. 1999. Linear *n*-point camera pose determination. *IEEE Transactions on Pattern Analysis and Machine Intelligence* 21, 8 (1999), 774–780.

Faith C. Robertson, Muhammad M. Abd-El-Barr, Srinivasan Mukundan, and William B. Gormley. 2017. Ventriculostomy-associated hemorrhage: A risk assessment by radiographic simulation. *Journal of Neurosurgery* 127, 3 (2017), 532–536.

Frank Sauer, Ali Khamene, Benedicte Bascle, and Gregory J. Rubino. 2001. A head-mounted display system for augmented reality image guidance: Towards clinical evaluation for iMRI-guided neurosurgery. In *Proceedings of the 4th International Conference on Medical Image Computing and Computer-Assisted Intervention*. 707–716.

Clemens M. Schirmer, J. Bradley Elder, Ben Roitberg, and Darlene A. Lobel. 2013. Virtual reality–based simulation training for ventriculostomy: An evidence-based approach. *Neurosurgery* 73, suppl. 1 (2013), S66–S73.

M. Scholz, W. Konen, S. Tombrock, B. Fricke, L. Adams, M. Von Duering, A. Hentsch, L. Heuser, and A. G. Harders. 1998. Development of an endoscopic navigation system based on digital image processing. *Computer Aided Surgery* 3, 3 (1998), 134–143.

Ramin Shahidi, Bai Wang, Marc Epitaux, Robert Grzeszczuk, and John Adler. 1998. Volumetric image guidance via a stereotactic endoscope. In *Proceedings of the International Conference on Medical Image Computing and Computer-Assisted Intervention.* 241–252.

Visish M. Srinivasan, Brent R. O'Neill, Diana Jho, Donald M. Whiting, and Michael Y. Oh. 2014. The history of external ventricular drainage: Historical vignette. *Journal of Neurosurgery* 120, 1 (2014), 228–236.

Philipp J. Stolka, Pezhman Foroughi, Matthew Rendina, Clifford R. Weiss, Gregory D. Hager, and Emad M. Boctor. 2014. Needle guidance using handheld stereo vision and projection for ultrasound-based interventions. In *Medical Image Computing and Computer-Assisted Intervention—MICCAI 2014*. Lecture Notes in Computer Science, Vol. 8647. Springer, 684–691.

Xuetong Sun and Amitabh Varshney. 2018. Investigating perception time in the far peripheral vision for virtual and augmented reality. In *Proceedings of the 15th ACM Symposium on Applied Perception (SAP'18)*. ACM, New York, NY, Article 13, 8 pages. DOI: https://doi.org/10.1145/3225153.3225160

Bruce L. Tai, Deborah Rooney, Francesca Stephenson, Peng-Siang Liao, Oren Sagher, Albert J. Shih, and Luis E. Savastano. 2015. Development of a 3D-printed external ventricular drain placement simulator. *Journal of Neurosurgery* 123, 4 (2015), 1070–1076.

Peter Y. M. Woo, Ben C. F. Ng, Jacob X. Xiao, Daniel Wong, Andrew Seto, Sandy Lam, Carmen Yim, et al. 2019. The importance of aspirin, catheterization accuracy, and catheter design in external ventricular drainage-related hemorrhage: A multicenter study of 1002 procedures. *Acta Neurochirurgica* 161, 8 (Aug. 2019), 1623–1632.

Rachel Yudkowsky, Cristian Luciano, Pat Banerjee, Alan Schwartz, Ali Alaraj, G. Michael Lemole Jr., Fady Charbel, et al. 2013. Practice on an augmented reality/haptic simulator and library of virtual brains improves residents' ability to perform a ventriculostomy. *Simulation in Healthcare* 8, 1 (2013), 25–31.

Received November 2018; revised July 2019; accepted October 2019